Noname manuscript No.
(will be inserted by the editor)

From elastic homogenization to upscaling of non-Newtonian fluid flows in porous media

Ruben Ibañez · Adrien Scheuer · Elena Lopez · Emmanuelle Abisset-Chavanne · Francisco Chinesta · Roland Keunings

Received: date / Accepted: date

Abstract Upscaling behaviors of heterogeneous microstructures to define macroscopic effective media is of major interest in many areas of computational mechanics, in particular those related to materials and processes engineering. In this paper, we explore the possibility of defining a macroscopic behavior manifold from microscopic calculations, and then use it directly for efficiently performing manifold-based simulations at the macroscopic scale. We consider in this work upscaling of non-Newtonian flows in porous media, and more particularly the ones involving short-fibre suspensions.

Keywords Permeability · Homogenization · Upscaling · Nonlinear fluids · Porous media · Manifold-based simulation

1 Introduction

In our recent work [14], we showed that it is possible to perform numerical simulations directly from data by circumventing, or at least alleviating, the necessity of considering a constitutive model to relate kinematic and dynamics variables. Thus, simulations proceed directly from the stress-strain data, from which standard discretization techniques proceed. In this paper, we perform a step forward in order to define macroscopic constitutive manifolds from the

R. Ibañez, A. Scheuer, E. Lopez, E. Abisset-Chavanne & F. Chinesta*
ICI Institute & ESI GROUP Chair
Centrale Nantes, 1 rue de la Noe, F-44300 Nantes, France
Tel.: + 33240376884
Fax: +33240372566
E-mail: Francisco.Chinesta@ec-nantes.fr
A. Scheuer & R. Keunings
ICTEAM, Université catholique de Louvain
Av. Georges Lemaitre 4, B-1348 Louvain-la-Neuve, Belgium
* Corresponding author Francisco Chinesta

microscopic calculations, and then solve the macroscopic mechanical problem from the data contained in these constitutive manifolds without having to determine explicitly an homogenized or upscaled constitutive equation.

In what follows we consider two scenarios, the first one related to linear or non-linear elasticity in heterogeneous media, while the second scenario concerns the flow of short-fibre suspensions in porous media.

When considering elastic models, where the different phases involved in the microstructure exhibit the same mechanical behaviour, whether linear or non-linear, homogenization is straightforward. Two main approaches exists, the hierarchical and the concurrent discussed in [8,11,19,16]. In the hierarchical approach micro and macro calculations are decoupled [3,30,21,10,25] whereas in the concurrent one both are strongly coupled [15,9,12,20,26,27,29,13].

On the other hand, when considering flows of simple or complex fluids in porous media, the situation becomes radically different because the physics encountered at the micro-scale differ from those postulated at the macro-scale. Thus, the micro-scale flow is governed by a Stokes flow problem, that becomes non-linear as soon as the fluid viscosity depends on the rate of strain. In the case of suspensions of rods (fibres, micro-fibres, nano-fibres or nanotubes), the micro-scale flow is governed by an anisotropic Stokes problem wherein viscosity is locally highly anisotropic. It is meaningless, however, to homogenize the microscopic flow parameters in order to define an effective viscosity at the macroscopic scale.

The standard macro-scale theoretical framework for flows in porous media is the Darcy model which relates averaged fluid velocities to pressure gradients. Being purely dissipative, the Darcy model cannot address elastic effects present in viscoelastic fluids. The same issue arises in modelling the flow of suspensions. While suitable evolution equations can be formulated for the micro-scale conformation, this cannot be achieved for averaged conformational quantities at the macro-scale.

In such circumstances, a possible route consists in defining a macroscopic flow model able to incorporate elastic effects for addressing viscoelastic fluids or an evolution equation for the upscaled conformation in the case of suspensions. Such a route, however, has two main handicaps: its intrinsic difficulty and its incompatibility with essentially all available simulation software used in industrial applications, which make use of Darcy's model.

Thus, the most valuable route consists in considering as much as possible viscous models that are more or less complex to capture the main fluid and flow features at the microscopic scale, and from them obtaining (by upscaling) an effective Darcy permeability at the macroscopic scale to be given as input to conventional simulation software. The main issue then is the calculation of the effective permeability. To do so, in this work as in many others, we enforce equality of the dissipated powers at both the micro and macro-scales.

In our former works [1,17,18], we followed that upscaling route successfully when considering purely viscous behaviors (Newtonian and generalized-Newtonian fluids) or by addressing viscoelastic behaviors from quasi-Newtonain

purely viscous formulations. In general, for non-linear behaviours, however, this approach quickly becomes very intricate and computationally expensive.

In the present paper, we follow a similar rationale, but instead of looking for an explicit expression of the effective permeability, we propose to build the so-called dissipation manifold, whose second derivative with respect to the macroscopic velocity directly yields the manifold of effective permeabilities.

2 Revisiting homogenization, upscaling and manifold-based macroscopic simulation

First, we consider the mechanical problem defined in a domain Ω occupied by a heterogeneous elastic material involving a number of phases evolving very fast spatially, thus allowing for scale separation. Even if the behaviour of each phase is assumed perfectly defined, the solution of the elastic problem in the whole domain requires a very fine discretization mesh for approximating the different fields (displacement, strain and stress) able to capture the microscopic details. To circumvent this difficulty, a widely considered approach consists in calculating the homogenized behaviour of the material by proceeding at the microscopic scale within the so-called representative volume element – RVE – ω, and then using these homogenized properties in the macroscopic calculation with a coarse mesh size larger than the characteristic length of the microstructure.

Assuming a linear elastic behaviour for each phase coexisting in the composite material, the Cauchy stress $\boldsymbol{\sigma}$ and strain $\boldsymbol{\epsilon}$ are related at each point $\mathbf{x} \in \omega$ by the constitutive model $\boldsymbol{\sigma} = \mathbf{c} : \boldsymbol{\epsilon}$, where $\mathbf{c}$ embodies the micro-scale elastic properties. Without loss of generality, the same microstructure is assumed everywhere in Ω. Thus, we can define the macroscopic strain $\mathbf{E}$ and stress $\boldsymbol{\Sigma}$ in ω according to the following spatial averages over the RVE:

$$\begin{cases} \mathbf{E} = \langle \boldsymbol{\epsilon} \rangle = \frac{1}{|\omega|} \int_\omega \boldsymbol{\epsilon}(\mathbf{x}) \, d\mathbf{x} \\ \boldsymbol{\Sigma} = \langle \boldsymbol{\sigma} \rangle = \frac{1}{|\omega|} \int_\omega \boldsymbol{\sigma}(\mathbf{x}) \, d\mathbf{x} \end{cases} . \tag{1}$$

Then, assuming the existence of a localization tensor $\mathbf{L}$ such that $\boldsymbol{\epsilon}(\mathbf{x}) = \mathbf{L}(\mathbf{x}) : \mathbf{E}$, we obtain

$$\boldsymbol{\Sigma} = \langle \boldsymbol{\sigma} \rangle = \langle \mathbf{c}(\mathbf{x}) : \boldsymbol{\epsilon}(\mathbf{x}) \rangle = \langle \mathbf{c}(\mathbf{x}) : \mathbf{L}(\mathbf{x}) \rangle : \mathbf{E}, \tag{2}$$

from which the homogenized elastic behavior $\mathbf{C}$ can be identified:

$$\mathbf{C} = \langle \mathbf{c}(\mathbf{x}) : \mathbf{L}(\mathbf{x}) \rangle. \tag{3}$$

The localization tensor can be computed in the linear case by solving three (in the 2D case) or six (in the 3D case) boundary value problems over ω, with affine displacements (that satisfy the Hill-Mandel principle) specified at the boundary $\partial\omega$ [4].

Obviously, the above rationale remains valid when the domain Ω contains different representative volume elements. It suffices to apply the procedure to each RVE, or in the limit case, at each evaluation point $\mathbf{X} \in \Omega$ (integration

point of the macroscopic discretized problem) by considering its associated microstructure $\omega(\mathbf{X})$.

In the non-linear case, the computational implementation is slightly more complex as the behaviour depends on the macroscopic strain, and consequently the elastic homogenized tensor is a function of the considered point $\mathbf{X} \in \Omega$ as soon as the macroscopic strain varies in Ω even if the microstructure remains the same everywhere in Ω.

From a methodological view point, we can assume the existence of a homogenized elastic tensor at each location $\mathbf{X} \in \Omega$. We could solve the non-linear elastic problem in the RVE attached to each Gauss point considered for discretizing the homogenized elastic problem at the macroscopic scale, by enforcing the displacement in agreement with the existing macroscopic strain at that location. Then, the elastic properties at each position $\mathbf{x} \in \omega(\mathbf{X})$ could be frozen in order to linearize the problem in ω before applying the rationale described above for homogenizing the linear behaviour.

The main drawback of this approach is the computational cost. It can be significantly alleviated by means of an alternative strategy based on the Proper Generalized decomposition (PGD) [5–7]. In [16], we proposed the calculation, for a given microstructure, of the parametric solution of the non-linear elastic problem in the REV for all feasible affine displacement enforced at its boundary.

A similar strategy was also successfully used in [18] when addressing the non-linear Stokes flow problem for a generalized-Newtonian fluid flowing in a porous medium. The resulting parametric local strain rates were used for determining the local parametric behaviour, and from it for obtaining the parametric solution of the boundary value problems, thus yielding a parametric localization tensor and from it the parametric upscaled Darcy behaviour.

Even though successful in these relatively simple problems, the above PGD procedure becomes very intricate to apply in more complex cases. In what follows, we develop an alternative approach that does not require the explicit evaluation of the homogenized or upscaled behaviours.

2.1 PGD-based generator of a macroscopic constitutive manifold

We consider a non-linear elastic problem defined in ω, and assume without loss of generality that the microstructure in ω represents the one existing everywhere in Ω. Within the PGD framework [5–7], we view the boundary conditions specified at $\partial\omega$ as model parameters and thus extra-coordinates of the problem.

Within the usual first-gradient elasticity framework, prescription of linear displacements at the boundary $\partial\omega$

$$\mathbf{u}(\mathbf{x} \in \partial\omega) = \begin{pmatrix} u_1 \\ u_2 \\ u_3 \end{pmatrix} = \begin{pmatrix} E_{11}x_1 + E_{12}x_2 + E_{13}x_3 \\ E_{12}x_1 + E_{22}x_2 + E_{23}x_3 \\ E_{13}x_1 + E_{23}x_2 + E_{33}x_3 \end{pmatrix}, \tag{4}$$

ensures the recovery of any macroscopic strain

$$\mathbf{E} = \begin{pmatrix} E_{11} & E_{12} & E_{13} \\ E_{12} & E_{22} & E_{23} \\ E_{13} & E_{23} & E_{33} \end{pmatrix}. \tag{5}$$

Within the PGD framework [5–7,16], the coefficients E_{ij} in (4) are viewed as extra-coordinates, and we seek the parametric solution

$$\mathbf{u}(\mathbf{x}, E_{11}, E_{12}, \cdots, E_{33}) \approx$$

$$\sum_{i=1}^{N} \mathbb{X}_i(\mathbf{x}) \circ \mathbb{E}_i^{11}(E_{11}) \circ \mathbb{E}_i^{12}(E_{12}) \circ \mathbb{E}_i^{13}(E_{13}) \circ \mathbb{E}_i^{22}(E_{22}) \circ \mathbb{E}_i^{23}(E_{23}) \circ \mathbb{E}_i^{33}(E_{33}), \tag{6}$$

where $\circ$ refers to the Hadamard product.

From the parametric displacement field (6), it is straightforward to compute the parametric strain and stress everywhere within ω, namely

$$\begin{cases} \boldsymbol{\epsilon}(\mathbf{x}, E_{11}, E_{12}, E_{13}, E_{22}, E_{23}, E_{33}) \\ \boldsymbol{\sigma}(\mathbf{x}, E_{11}, E_{12}, E_{13}, E_{22}, E_{23}, E_{33}) \end{cases}, \tag{7}$$

from which macroscopic strain as stress, $\mathbf{E}$ and $\boldsymbol{\Sigma}$ respectively, can be obtained from Eq. (1). As just indicated $\mathbf{E}$ is directly given by Eq. (5).

The macroscopic constitutive manifold $\boldsymbol{\Sigma}(\mathbf{E})$ is then defined by

$$\boldsymbol{\Sigma}(\mathbf{E}) \;=\; \langle \boldsymbol{\sigma}(\mathbf{x}, E_{11}, E_{12}, E_{13}, E_{22}, E_{23}, E_{33}) \rangle. \tag{8}$$

Now, as many macroscopic strain-stress couples $(\boldsymbol{\Sigma}_m, \mathbf{E}_m)$, $m = 1, \ldots, M$ can be generated in real time by simply particularizing the parametric solution (8). Each stress-strain couple is a single point $\mathbf{P}_m$ in a space of dimension $D = 12$ (the six distinct components of the stress and strain tensors, respectively). In the sequel, we use Voigt's notation, i.e. stress and strain tensors will be represented as vectors and consequently the fourth-order elastic tensor reads as a 6×6 square matrix.

Each vector $\mathbf{P}_m$ thus defines a point in a space of dimension D and, therefore, the whole set of stress-strain couples is a set of M points in $\mathbb{R}^D$. We conjecture that all these sample points belong to a low-dimensional manifold embedded in the high-dimensional space $\mathbb{R}^D$, thus allowing for a non-linear dimensionality reduction as discussed in [14]. In what follows, however, we proceed without such a dimensionality reduction and use the simplest strategy proposed and discussed in [14]. We consider locally-linear approximations, that allow us to write

$$\mathbf{P}_m = \sum_{i=1}^{M} W_{mi} \mathbf{P}_i, \tag{9}$$

with $W_{mi} = 0$ if $i \notin \mathcal{S}_m$, being $\mathcal{S}_m$ the set containing the K-nearest neighbours of $\mathbf{P}_m$. By minimizing the functional

$$\mathcal{H}(\mathbf{C}) = \sum_{i \in \mathcal{S}_m} (\boldsymbol{\Sigma}_i - \mathbf{C} \cdot \mathbf{E}_i)^2, \tag{10}$$

we obtain the locally-linear behaviour $\mathbf{C}(\mathbf{P}_m) \equiv \mathbf{C}_m$.

2.2 Manifold-based simulation

Once the locally-linear behaviour $\mathbf{C}(\mathbf{P})$ is identified, we may apply the simplest linearization technique operating on the standard weak form

$$\int_{\Omega} \mathbf{E}^*(\mathbf{X}) : \boldsymbol{\Sigma}(\mathbf{X})\ d\mathbf{X} = \int_{\Gamma_N} \mathbf{U}^*(\mathbf{X}) \cdot \mathbf{T}(\mathbf{X})\ d\mathbf{X}, \tag{11}$$

where at each point, from the stress-strain couple $\mathbf{P}(\mathbf{X})$ at position $\mathbf{X}$, the locally-linear behaviour $\mathsf{C}(\mathbf{P}(\mathbf{X}))$ can be obtained (i.e. in practice, at the Gauss points used for the integration of the weak form). We thus have, using Voigt's notation,

$$\int_{\Omega} \mathbf{E}^*(\mathbf{X}) \cdot (\mathbf{C}(\mathbf{X})\mathbf{E}(\mathbf{X}))\, d\mathbf{X} = \int_{\Gamma_N} \mathbf{U}^*(\mathbf{X}) \cdot \mathbf{T}(\mathbf{X})\ d\mathbf{X}. \tag{12}$$

This allows us, in turn, to obtain the displacement field and from it, to update the strain and stress fields, to compute again the updated locally-linear behaviour. The process continues until convergence [14].

3 Non-linear viscous fluids in porous media: manifold-based upscaling

Isothermal flows of non-linear fluids in complex microstructures can be simulated by solving the momentum and mass balance equations and a suitable rheological constitutive model. For inertialess incompressible flows, these balance equations read,

$$\nabla \cdot \boldsymbol{\sigma} = \mathbf{0}, \tag{13}$$

and

$$\nabla \cdot \mathbf{v} = 0. \tag{14}$$

Here, $\boldsymbol{\sigma}$ is the Cauchy stress tensor and $\mathbf{v}$ the velocity field, both defined at time t at each point within the fluid domain Ω_f. When considering porous media, the domain Ω is assumed fully saturated, with the fluid phase occupying the region Ω_f whereas the remaining part $\Omega_s = \Omega - \Omega_f$ is occupied by a solid phase assumed at rest.

An appropriate constitutive equation must be postulated to describe the fluid's rheology. There are many possible choices, the most usual ones being related to Newtonian, generalized-Newtonian and quasi-Newtonian fluids, as well as to suspensions, briefly summarized below:

- *Newtonian fluid.* For a Newtonian fluid, the constitutive equation reads

  $$\boldsymbol{\sigma} = -p\mathbf{I} + \boldsymbol{\tau} = -p\mathbf{I} + 2\eta\mathbf{D}, \tag{15}$$

  where p is the pressure field that can be interpreted as the Lagrange multiplier associated with the incompressibility constraint, $\mathbf{I}$ is the identity tensor, $\boldsymbol{\tau}$ the extra-stress tensor, η the constant fluid viscosity and $\mathbf{D}$ the rate of strain tensor, i.e. the symmetric part of the velocity gradient, $2\mathbf{D} = \nabla\mathbf{v} + (\nabla\mathbf{v})^T$.

– *Generalized-Newtonian fluid.* For a generalized-Newtonian fluid, the constitutive equation (15) remains formally unchanged, but a viscosity η that depends on the effective strain rate $\dot{\gamma}$. The latter is usually expressed from the second invariant of the rate of strain tensor, i.e. $\dot{\gamma} = \sqrt{2\mathbf{D} : \mathbf{D}}$. The simplest of such models is the power-law viscosity given by

$$\eta = \kappa \dot{\gamma}^{n-1}, \tag{16}$$

where κ and n are the consistency and power-law index, respectively. The value $n = 1$ corresponds to a Newtonian fluid.

– *Quasi-Newtonian fluid.* In the quasi-Newtonian fluid model, the viscosity function is not merely a function of the second invariant of the rate of strain tensor but also depends on the relative rate of rotation of the fluid. Consequently, the quasi-Newtonian fluid is able to show e.g. shear-thinning in shear flow and extension-thickening in elongational flow. The constitutive equation for the quasi-Newtonian fluid reads

$$\boldsymbol{\sigma} = -p\mathbf{I} + 2\eta_{QN}\mathbf{D}, \tag{17}$$

where η_{QN} is the effective viscosity of the fluid that accounts for shear as well as extension according to the local type of flow. The latter is quantified by means of a scalar quantity χ that differentiates the type of regime (shear, elongation or rigid motion) [23,28]. In [23] for example, the following viscosity function is proposed for 2D planar flows:

$$\eta_{QN}(\dot{\gamma}, \chi) = \left(\eta_S(\dot{\gamma})\right)^{f(\chi)} \left(\eta_E(\dot{\epsilon})\right)^{1-f(\chi)}, \tag{18}$$

with the shear viscosity η_S depending on $\dot{\gamma}$ (as in the case of generalized-Newtonian fluids) and the extensional viscosity η_E depending on $\dot{\epsilon}$, with $2\dot{\epsilon} = \dot{\gamma}$, and with the function $f(\chi)$ satisfying

$$f(\chi) = \begin{cases} 1, \text{ if } \chi = 1 \\ 0, \text{ if } \chi = 0 \end{cases}, \tag{19}$$

in order to recover the shear viscosity at locations exhibiting a shear flow and the extensional viscosity where planar extension occurs. We consider $f(1 < \chi \leq 2) = 1$ for approaching the zero shear rate viscosity in the limit case of rigid rotation.

– *Suspension of rigid rods in a Newtonian fluid.* When considering a population of rigid rods immersed into a Newtonian fluid, and making use of suitable simplifying assumptions [2], the constitutive equation for the suspension reads

$$\boldsymbol{\sigma} = -p\mathbf{I} + 2\eta\mathbf{D} + 2\eta N_p(\mathbf{a} : \mathbf{D})\mathbf{a}, \tag{20}$$

where $\mathbf{a}$ is the so-called orientation tensor and N_p is a material parameter. The evolution of $\mathbf{a}$ is governed by the Folgar & Tucker model

$$\dot{\mathbf{a}} = \nabla\mathbf{v} \cdot \mathbf{a} - \mathbf{a} \cdot (\nabla\mathbf{v})^T - 2(\mathbf{a} : \mathbf{D})\mathbf{a} + \beta\left(\mathbf{a} - \frac{\mathbf{I}}{3}\right). \tag{21}$$

In view of the advective character of this equation, suitable boundary conditions must be specified for $\mathbf{a}$ at the inflow boundary of the RVE only, whereas velocity boundary conditions must be specified on the whole boundary.

3.1 Upscaling non-Newtonian fluids flowing in porous media

The flow model is solved in the representative volume $\omega(\mathbf{X})$, where two phases coexist, i.e. the fluid phase occupying the domain $\omega_f(\mathbf{X})$ and the solid phase, assumed rigid and at rest, occupying the region $\omega_s(\mathbf{X})$, with $\omega_f(\mathbf{X}) \cup \omega_s(\mathbf{X}) = \omega(\mathbf{X})$ and $\omega_f(\mathbf{X}) \cap \omega_s(\mathbf{X}) = \emptyset$. The flow model consists of the mass and momentum balance equations complemented by the constitutive equation discussed in the previous section, namely

$$\begin{cases} \nabla \cdot \boldsymbol{\sigma} = \mathbf{0} \\ \nabla \cdot \mathbf{v} = 0 \\ \boldsymbol{\sigma} = -p\mathbf{I} + \boldsymbol{\tau} \end{cases}. \tag{22}$$

Here, $\boldsymbol{\tau} = \boldsymbol{\tau}(\mathbf{D})$ in the case of Newtonian, generalized-Newtonian and quasi-Newtonian fluids and $\boldsymbol{\tau} = \boldsymbol{\tau}(\mathbf{D}, \mathbf{a})$ in the case of rod suspensions.

The above governing equations are complemented with the boundary condition $\mathbf{v}(\mathbf{x} \in \partial\omega(\mathbf{X})) = \mathbf{V}$, where $\mathbf{V}$ comes from the macroscopic flow problem.

The solution of the flow problem (22) yields the velocity field $\mathbf{v}(\mathbf{x} \in \omega_f(\mathbf{X}))$, and from it the strain rate $\mathbf{D}(\mathbf{x} \in \omega_f(\mathbf{X}))$.

One can thus compute the power $\mathcal{DP}(\mathbf{V}; \mathbf{X})$ dissipated in the RVE and associated with the macroscopic velocity $\mathbf{V}$ prescribed at the boundary $\partial\omega$:

$$\mathcal{DP}(\mathbf{V}; \mathbf{X}) = \int_{\omega_f(\mathbf{X})} \boldsymbol{\sigma}(\mathbf{x}) : \mathbf{D}(\mathbf{x}) d\mathbf{x}. \tag{23}$$

The specific microscopic dissipation $\mathcal{DP}^m$ is then obtained by dividing $\mathcal{DP}$ given by (23) by the RVE volume $|\omega(\mathbf{X})|$.

Obviously, the considered fluid models being purely viscous, they only involve dissipated power, and consequently the effective macroscopic model should account for it. In Darcy's model, the specific macroscopic dissipated power $\mathcal{DP}^M$ reads

$$\mathcal{DP}^M(\nabla P, \mathbf{V}) = \nabla P \cdot \mathbf{V}. \tag{24}$$

Thus, by equating the micro and macro-scale dissipations, we obtain

$$\mathcal{DP}^m = \nabla P|_{\mathbf{X}} \cdot \mathbf{V}(\mathbf{X}), \tag{25}$$

or by assuming the existence of an effective permeability $\mathbf{K}_{eff}(\mathbf{X})$,

$$\nabla P|_{\mathbf{X}} = \mathbf{K}_{eff}^{-1}(\mathbf{X}) \mathbf{V}(\mathbf{X}), \tag{26}$$

from which we finally obtain our main result:

$$\mathcal{DP}^m(\mathbf{V}; \mathbf{X}) = \mathbf{K}_{eff}^{-1}(\mathbf{X}) : (\mathbf{V}(\mathbf{X}) \otimes \mathbf{V}(\mathbf{X})). \tag{27}$$

This expression constitutes a constructive definition of the effective permeability. For calculating the latter, it suffices to take the second derivative of $\mathcal{DP}^m(\mathbf{V})$ related to the microstructure existing at location $\mathbf{X}$:

$$\mathbf{K}_{eff}^{-1}(\mathbf{X}) = \frac{1}{2} \frac{d^2 \mathcal{DP}^m(\mathbf{V}; \mathbf{X})}{d\mathbf{V}^2}. \tag{28}$$

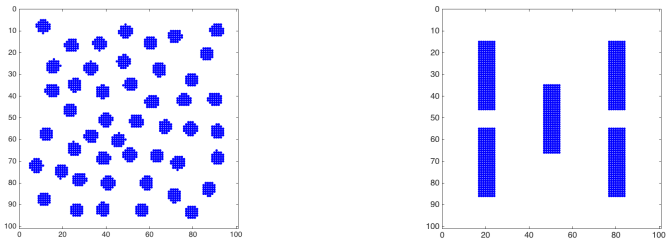

Fig. 1 RVE for two microstructures: isotropic (left) and orthotropic (right)

We note that for a Newtonian fluid, the velocity, strain-rate and stress fields scale linearly with the velocity prescribed at the RVE boundary. Thus, the dissipated power scales with the square of the velocity, leading to a constant effective permeability [17].

Thus, micro-macro simulations can be performed very efficiently. After solving at a given iteration the macroscopic flow problem, from the computed velocity $\mathbf{V}$ at each macroscopic location $\mathbf{X}$, the associated permeability can be updated according to Eq. (28). This calculation is performed in almost real-time. From the updated permeability, a new macroscopic calculation can be carried out.

4 Numerical examples

We consider two different microstructures, i.e. isotropic and orthotropic, as depicted in Fig. 1.

4.1 Upscaling Newtonian fluids flowing in porous media

The specific dissipated power $\mathcal{DP}^M$ obtained for a Newtonian fluid is shown in Figs. 2 and 3 for the isotropic and anisotropic microstructures, respectively.

In view of (28), the components of the effective permeability tensor are obtained by taking the second derivatives of the dissipated power with respect to the velocity $\mathbf{V}$ prescribed at the RVE boundary, and inverting the resulting matrix. As discussed in [17], the intrinsic permeability obtained for a Newtonian fluid is a purely geometrical property and can be obtained by multiplying the effective permeability by the viscosity.

Figures 4 and 5 depict the components of the effective permeability for a Newtonian fluid flowing in the isotropic and anisotropic microstructures shown in Fig. 1, respectively. It can be noticed that the permeability does not depend on the prescribed velocity in view of the linear behaviour of the fluid. Moreover, for the almost isotropic microstructure, as expected, the diagonal components of the permeability tensor are quite similar, whereas the off-diagonal component is much smaller. For the orthotropic microstructure, a clear difference

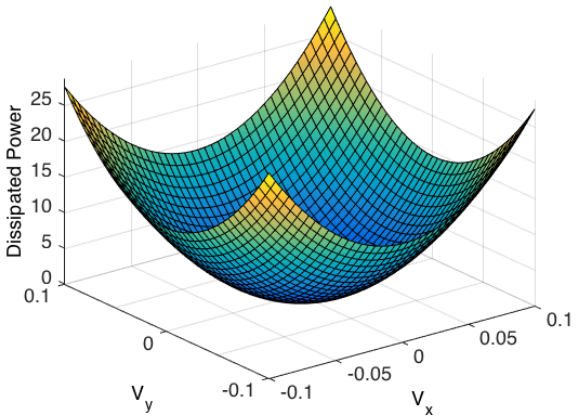

Fig. 2 Specific dissipated power for a Newtonian fluid flowing in the isotropic microstructure depicted in Fig. 1 (left)

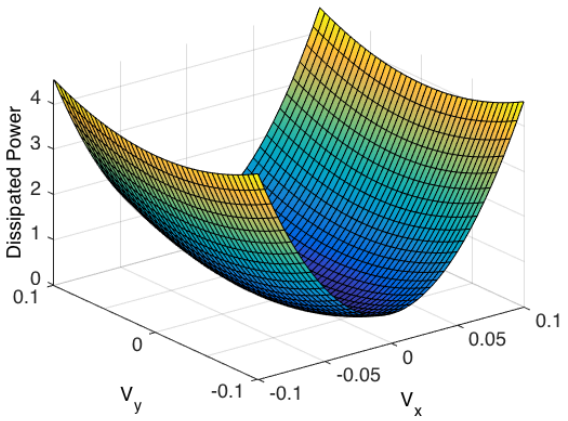

Fig. 3 Specific dissipated power for a Newtonian fluid flowing in the orthotropic microstructure depicted in Fig. 1 (right)

is noticed between the diagonal components, and the off-diagonal component vanishes. Indeed, the microstructure perfectly aligns with the coordinates axes that constitute the principal directions of the permeability tensor.

For the generalized-Newtonian and quasi-Newtonian fluid models, the results obtained using the proposed procedure based on the dissipated power manifold are, as expected, in excellent agreement with the ones obtained using the analytical procedure described in our former works [1,18].

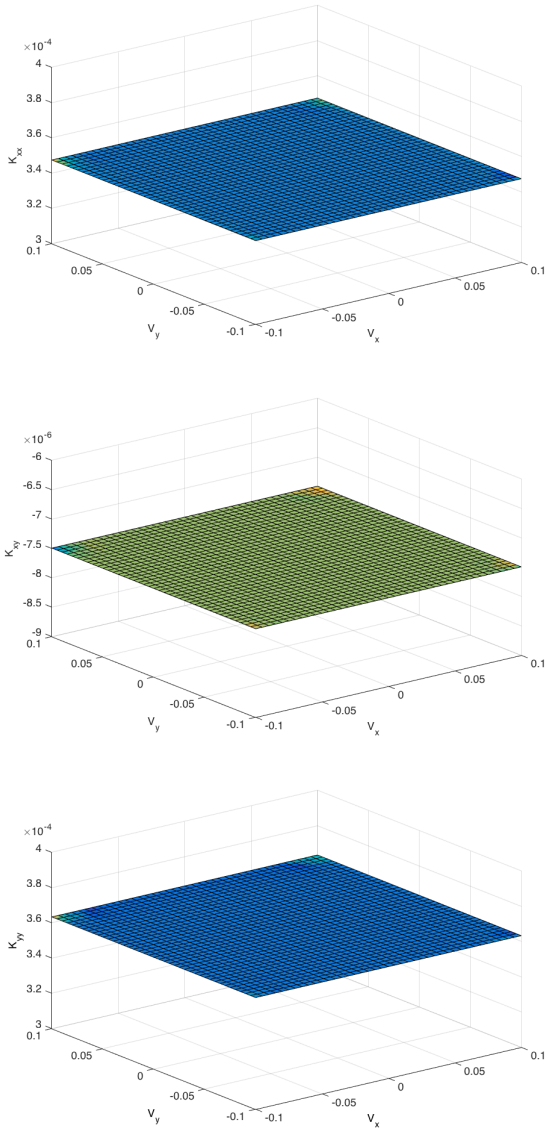

Fig. 4 Newtonian fluid and isotropic microstructure. Components of the effective permeability tensor: K_{xx} (top), K_{xy} (middle) and K_{yy} (bottom)

4.2 Upscaling suspensions of rods flowing in porous media

As detailed in Section 3, the flow model for a suspension of rods consists of the momentum and mass balances complemented with the constitutive equation

$$\boldsymbol{\sigma} = -p\mathbf{I} + 2\eta\mathbf{D} + 2\eta N_p(\mathbf{a} : \mathbf{D})\mathbf{a}, \tag{29}$$

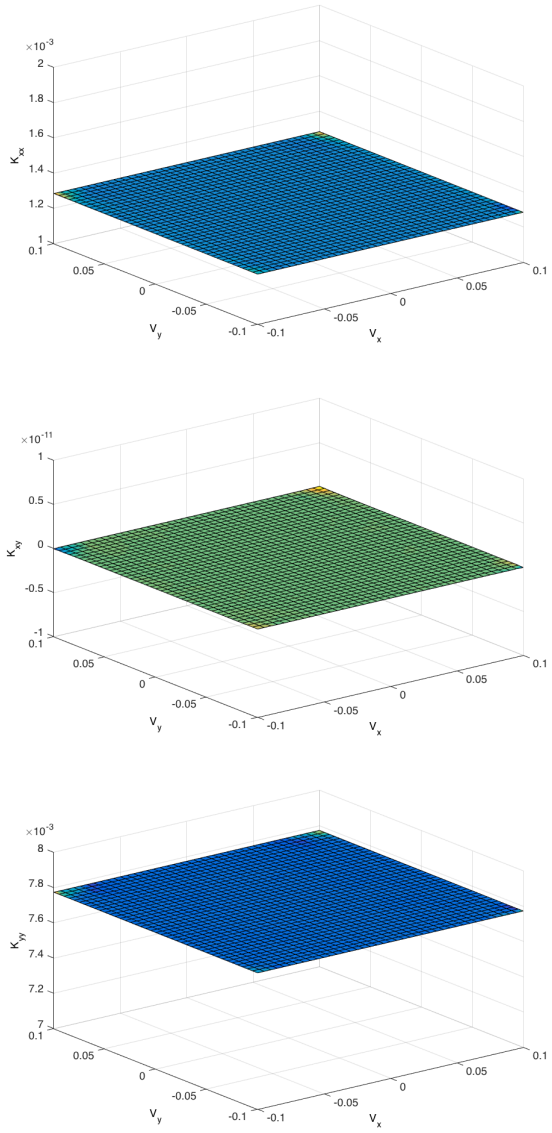

Fig. 5 Newtonian fluid and orthotropic microstructure. Components of the effective permeability tensor: K_{xx} (top), K_{xy} (middle) and K_{yy} (bottom)

that involves the conformation tensor $\mathbf{a}$ whose evolution is governed by the transport equation

$$\dot{\mathbf{a}} = \nabla \mathbf{v} \cdot \mathbf{a} - \mathbf{a} \cdot (\nabla \mathbf{v})^T - 2(\mathbf{a} : \mathbf{D})\mathbf{a} + \beta \left(\mathbf{a} - \frac{\mathbf{I}}{3} \right). \tag{30}$$

The resulting flow problem is solved in the RVE ω with the macroscopic velocity $\mathbf{V}$ specified at the RVE boundary $\partial\omega$. In order to solve the orientation equation (30), one must specify the orientation tensor at the inflow boundary $\partial^-\omega \subset \partial\omega$ characterized by $\mathbf{V}\cdot\mathbf{n}(\mathbf{x}\in\partial\omega) < 0$, where $\mathbf{n}$ is the outward unit vector normal to $\partial\omega$ at point $\mathbf{x}$.

The need for these inflow conditions is a really difficult issue. Indeed, while we can naturally define at the macroscopic scale an upscaled orientation tensor $\mathbf{A} \equiv \langle\mathbf{a}\rangle$, we cannot formulate a proper evolution equation for $\mathbf{A}$ at the macroscopic scale in terms of the averaged velocities $\mathbf{V}$ appearing in the Darcy model. The orientation evolution is induced and driven by the local velocity gradients existing at the microscopic scale. It is assumed that the characteristic fibers length is lower than the characteristic channels diameter in order to neglect confinement effects addressed in [22,24].

When solving the micro-scale flow problem, the orientation to be prescribed at the inflow boundary $\partial^-\omega$ is in fact undetermined. In order to quantify the impact of this indeterminacy, we decided to specify arbitrary orientation states at $\partial^-\omega$. In view of the intense tortuosity that complex microstructures entail, we found that the orientation field rapidly forgets its entrance condition (fading memory) and is essentially velocity-driven. Thus, the micro-scale solution depends almost exclusively on the prescribed velocity $\mathbf{V}$ that arises from the macroscopic scale. This empirical observation is of crucial importance.

In the case of intense randomizing effects the solution will become almost isotropic and again independent of the enforced orientation on the inflow boundary.

In practice, any orientation can thus be prescribed at the inflow boundary $\partial^-\omega$, the simplest ones being: (i) an isotropic orientation state $\mathbf{a}(\mathbf{x}\in\partial^-\omega) = \mathbf{I}/2$ or $\mathbf{I}/3$ in the 2D or 3D cases, respectively; (ii) the local alignement of rods with the incoming flow, $\mathbf{a}(\mathbf{x}\in\partial^-\omega) = (\mathbf{V}\otimes\mathbf{V})/\|\mathbf{V}\|^2$; or the macroscopic orientation existing at that position at the previous iteration, $\mathbf{a}(\mathbf{x}\in\partial^-\omega) = \hat{\mathbf{A}}$. Thus, with the macroscopic velocity $\mathbf{V}$ specified on the whole boundary $\partial\omega$ and the orientation at the inflow boundary $\partial^-\omega$, the micro-scale flow problem is solved to obtain $\mathbf{v}(\mathbf{x})$, $\mathbf{D}(\mathbf{x})$, $\boldsymbol{\tau}(\mathbf{x})$ and $\mathbf{a}(\mathbf{x})$ at each position $\mathbf{x}$ in the fluid domain ω_f, and from those, the dissipated power $\mathcal{DP}$ and the averaged orientation $\mathbf{A} = \langle\mathbf{a}(\mathbf{x})\rangle$.

Since the outputs of the microscopic calculation are almost entirely velocity-driven, we can assume the existence of the two manifolds $\mathcal{DP}(\mathbf{V})$ and $\mathbf{A}(\mathbf{V})$. The first manifold yields the effective permeability, while the second gives a macroscopic descriptor of the orientation field.

Figure 6 compares the components of the macroscopic orientation tensor $\mathbf{A}$ as a function of the prescribed velocity $\mathbf{V}$, obtained for the isotropic and orthotropic microstructures of Fig. 1. The expected symmetries are noticed for the isotropic microstructure, while a preferential orientation along the y-direction is predicted in the orthotropic case.

Unlike for a Newtonian fluid, the effective permeability of the suspension does depend on the prescribed velocity $\mathbf{V}$, in view of the non-linearity of the micro-scale problem. This can be seen in the results shown in Fig. 7, obtained

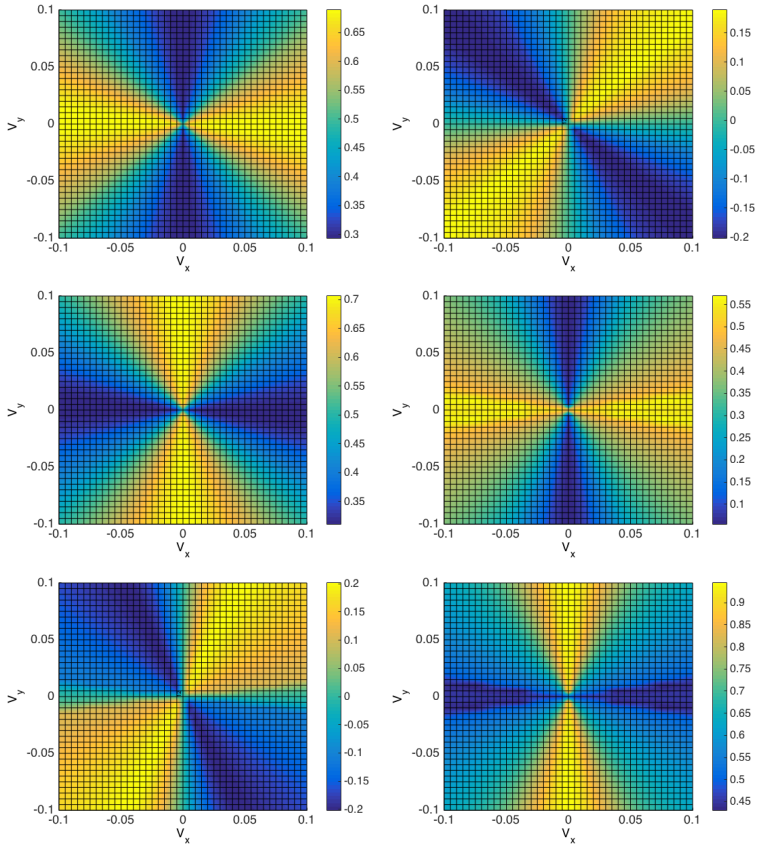

Fig. 6 Components of the upscaled orientation tensor $\mathbf{A}$ (A_{xx} in the left, A_{xy} in the center and A_{yy} in the right) for the isotropic (top) and orthotropic (bottom) microstructures (the colour-bar is different in each graph)

for the isotropic microstructure. Comparison with the Newtonian results shows that the presence of rods yields an overall decrease of the effective permeability.

5 Conclusions

This paper explored the possibility of performing manifold-based upscaling of linear and non-linear models for flows in porous media. We proposed the construction of the so-called dissipated power manifold whose second derivative with respect to the macroscopic velocity (enforced at the boundary of the RVE) yields the inverse of the effective permeability tensor. When solving the micro-scale problem parametrically by means of the PGD, construction of the dissipated power manifold is straightforward and extremely fast from the computational point of view.

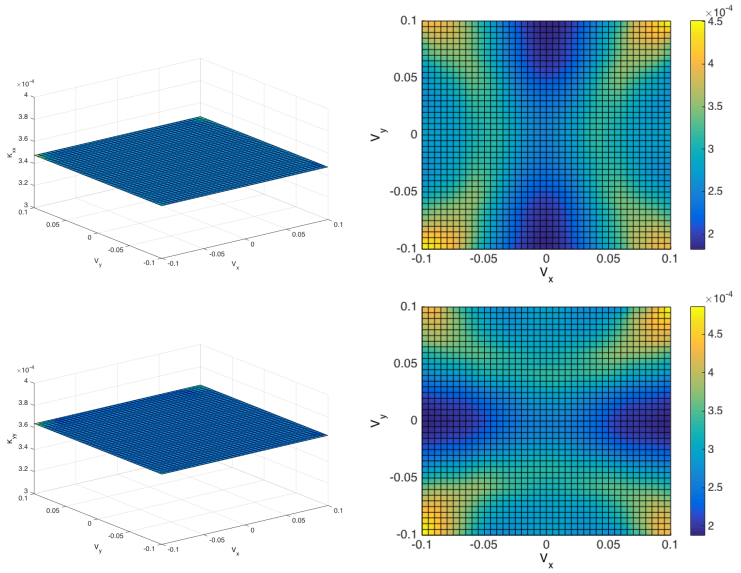

Fig. 7 Isotropic microstructure: comparing the effective permeability components K_{xx} (top) and K_{yy} (bottom) for a Newtonian fluid (left) and a suspension of rods (right)

The second contribution of the present paper is the consideration of suspensions of rods flowing in porous media. Through numerical experiments, we found that the dissipated power is insensitive to the orientation state that must be specified at the inflow boundary of the RVE, and thus mostly depends on the macroscopic velocity prescribed at the RVE boundary. This crucial observation allowed us to apply the proposed upscaling procedure to complex fluids endowed with a fading memory.

Compliance with Ethical Standards. The authors declare that they have no conflict of interest.

References

1. A. Ammar, E. Abisset-Chavanne, F. Chinesta, R. Keunings. Flow modelling of quasi-Newtonian fluids in two-scale fibrous fabrics. Advanced simulations. International Journal of Material Forming, In press.
2. C. Binetruy, F. Chinesta, R. Keunings. Flows in Polymers, Reinforced Polymers and Composites. A multiscale approach. Springerbriefs, Springer, 2015.
3. H.J. Bőhm. A Short Introduction to Basic Aspects of Continuum Micromechanics. ISLB Report 208, TU Wien, Vienna, http://www.ilsb.tuwien.ac.at/links/downloads/ilsbrep206.pdf, 2009.
4. F. Chinesta, A. Ammar, F. Lamarchand, P. Beauchene, F. Boust. Alleviating mesh constraints: Model reduction, parallel time integration and high resolution homogenization. Computer Methods in Applied Mechanics and Engineering, 197, 400-413, 2008.

5. F. Chinesta, A. Ammar, A. Leygue, R. Keunings. An Overview of the Proper Generalized Decomposition with Applications in Computational Rheology. Journal of Non Newtonian Fluid Mechanics, 166, 578-592, 2011.
6. F. Chinesta, A. Leygue, F. Bordeu, J.V. Aguado, E. Cueto, D. Gonzalez, I. Alfaro, A. Ammar, A. Huerta. Parametric PGD based computational vademecum for efficient design, optimization and control. Archives of Computational Methods in Engineering, 20/1, 31-59, 2013.
7. F. Chinesta, R. Keunings, A. Leygue, The Proper Generalized Decomposition for Advanced Numerical Simulations: A Primer, Springerbriefs, Springer, 2014.
8. R. de Borst. Challenges in computational materials science: Multiple scales, multi-physics and evolving discontinuities. Computational Materials Science, 43/1, 1-15, 2008.
9. F. Feyel. Multiscale FE2 elastoviscoplastic analysis of composite structures. Computational Materials Science, 16/1-4, 344-354, 1999.
10. J. Fish, Z. Yuan. Multiscale enrichment based on partition of unity. International Journal for Numerical Methods in Engineering, 62/10, 1341-1359, 2005.
11. J. Fish. Bridging the scales in nano engineering and science,.Journal of Nanoparticle Research, 8/5, 577-594, 2006.
12. M.G.D. Geers, V.G. Kouznetsova, W.A.M. Brekelmans. Multi-scale computational homogenization: Trends and challenges. Journal of Computational and Applied Mathematics, 234/7, 2175-2182, 2010.
13. F. E. Halabi, D. González, A. Chico, M. Doblaré. FE^2 multiscale in linear elasticity based on parametrized microscale models using proper generalized decomposition. Computer Methods in Applied Mechanics and Engineering, 257, 183 - 202, 2013.
14. R. Ibanez, E. Abisset-Chavanne, J.V. Aguado, D. Gonzalez, E. Cueto, F.Chinesta. A manifold learning approach to data-driven computational elasticity and inelasticity, Archives of Computational Methods in Engineering, DOI 10.1007/s11831-016-9197-9, 2016
15. P. Kanouté, D.P. Boso, J.L. Chaboche, B.A. Schrefler. Multiscale Methods for Composites: A Review. Archives of Computational Methods in Engineering, 16/1, 31-75, 2009.
16. H. Lamari, A. Ammar, P. Cartraud, G. Legrain, F. Jacquemin, F. Chinesta. Routes for Efficient Computational Homogenization of Non-Linear Materials Using the Proper Generalized Decomposition. Archives of Computational Methods in Engineering, 17/4, 373-391, 2010.
17. E. Lopez, E. Abisset-Chavanne, S. Comas-Cardona, C. Binetruy et F. Chinesta. Flow modeling of linear and nonlinear fluids in two and three scale fibrous fabrics. International Journal of Material Forming. In press.
18. E. Lopez, A. Leygue, E. Abisset-Chavanne, S. Comas-Cardona, C. Aufrere, C. Binetruy, F. Chinesta. Flow modeling of linear and nonlinear fluids in two scale fibrous fabrics. Advanced simulations. International Journal of Material Forming, In press.
19. C. McVeigh, W.K Liu, Linking microstructure and properties through a predictive multiresolution continuum. Computer Methods in Applied Mechanics and Engineering, 197/41-42, 3268-3290, 2008.
20. J.C. Michel, P. Suquet. Computational analysis of nonlinear composite structures using the nonuniform transformation field analysis. Computer Methods in Applied Mechanics and Engineering, 193/48-51, 5477-5502, 2004.
21. A. Mobasher-Amini, D. Dureisseix, P. Cartraud. Multi-scale domain decomposition method for large-scale structural analysis with a zooming technique: Application to plate assembly. International Journal for Numerical Methods in Engineering, 79/4, 417-443, 2009.
22. M. Perez, A. Scheuer, E. Abisset-Chavanne, F. Chinesta, R. Keunings. A multi-scale description of orientation in confined suspensions involving rods. Journal of Non-Newtonian Fluid Mechanics, 233, 61-74, 2016.
23. E. Ryssel, P.O. Brunn. Comparison of a quasi-Newtonian fluid with a viscoelastic fluid in planar contraction flow. J. Non-Newtonian Fluid Mech., 86, 309-335, 1999.
24. A. Scheuer, E. Abisset-Chavanne, F. Chinesta, R. Keunings. Second-gradient modelling of orientation development and rheology of confined suspensions. Journal of Non-Newtonian Fluid Mechanics, 237, 54-64, 2016.

25. T. Strouboulis, L. Zhang, I. Babuška. p-version of the generalized FEM using mesh-based handbooks with applications to multiscale problems. International Journal for Numerical Methods in Engineering, 60/10, 1639 - 1672, 2004.
26. I. Temizer, P. Wriggers. An adaptive method for homogenization in orthotropic nonlinear elasticity. Computer Methods in Applied Mechanics and Engineering, 196/35-36, 3409-3423, 2007.
27. I. Temizer, T. Zohdi, A numerical method for homogenization in non-linear elasticity. Computational Mechanics. 40/2, 281-298, 2007.
28. R.L. Thompson, P.R. Souza Mendes. Persistence of straining and flow classification. International Journal of Engineering Science, 43, 79-105, 2005.
29. J. Yvonnet, D. Gonzalez, Q.-C. He. Numerically explicit potentials for the homogenization of nonlinear elastic heterogeneous materials. Computer Methods in Applied Mechanics and Engineering, 198/33-36, 2723-2737, 2009.
30. T. Zohdi, P. Wriggers,.An Introduction to Computational Micromechanics, Springer, 2005.